Supplementary Material (ESI) for Green Chemistry

Supporting Information

In-Situ Spectroscopic Investigation of the Cobalt-Catalyzed Oxidation of Lignin Model Compounds in Ionic Liquids

Joseph Zakzeski, Pieter C. A. Bruijnincx, and Bert M. Weckhuysen*[a]

---

[a] Dr. J. Zakzeski, Dr. P. C. A. Bruijnincx, Prof. dr. ir. B. M. Weckhuysen
Inorganic Chemistry and Catalysis group
Debye Institute for Nanomaterials Science
Utrecht University
Sorbonnelaan 16, 3584 CA Utrecht, The Netherlands
Fax: (+31 30 251 1027)
E-mail: b.m.weckhuysen@uu.nl

Table of Contents:

Figure S20. Vibrational intensities associated with ^{16}O (1683 cm^{-1}) and ^{18}O (1657 cm^{-1}) labelled veratraldehyde versus time using $^{18}O_2$ as the oxidant.

Figure S21: In-situ IR spectrum of Co/[EMIM][DEP]/OH catalyzed veratryl alcohol oxidation using $^{18}O_2$ for comparison with Figure 2. Vibrations associated with cobalt complexes are marked with arrows.

Scheme S1: Proposed catalytic mechanism depicting the exemplary oxidation of veratryl alchol to veratraldehyde in the ionic liquid [EMIM][DEP] using $^{18}O_2$ as the oxidant.

Supporting Information References

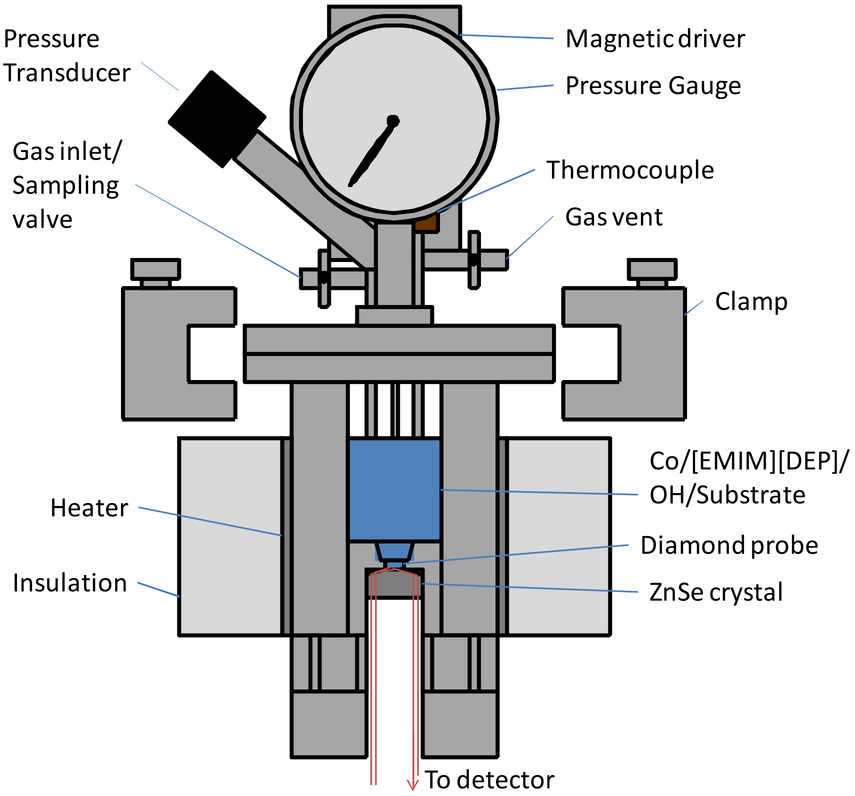

Figure S1: Schematic depiction of the ATR-IR apparatus.

Table S1. IR and Raman bands of [EMIM][DEP] and their vibrational assignments. Asym = antisymmetric, sym = symmetric, str = stretch, ip = in-plane, op = out-of-plane, sh = shoulder.

Infrared (cm^{-1})	Relative Intensity	Raman (cm^{-1})	Vibrational assignment
		3159	Ring HCCH asym str
3147	7		Ring HCCH sym str
3046	17	3070	CH_3(N) HCH asym str
2975	32	2973	CH_2 HCH asym str
2934	22	2931	Terminal CH_3 HCH asym str
2889	90	2890	Terminal CH_3 HCH sym str
2826	9sh	2837	?
2755	5	2759	?
2732	4	2714	?
1717	5		?
1679	5	1568	C=C str
1571	26	1482	C=N str
1470	15sh	1456	Ring ip asym str, CH3(N) str
1457	18	1388	CCH HCH asym bend, CH_3(N) HCH sym bend
1385	23		Ring ip asym str, CH_2(N) bend
1362	12	1337	Ring ip sym str, CH_2(N) str
1336	11	1279	P=O str
1243	89		Ring ip asym str, CC str, (N)CH_2 and (N)CH_3CN str
1179	49	1123	CC str
1105	40	1089	PO_2^- sym str
1082	69	1058	Ring sym str, CH_3(N) str, CH_2(N) str
1060	99	1021	P-O-C vibration

1049	100	959	CC str
960	24sh	939	P-O-C vibration
933	76	811	CCH bend
806	40sh	785	P-O-C sym str
776	87	748	Ring HCCH asym bend
728	56	731	Ring HCCH sym bend
706	29sh	704	Ring ip bend, CH_3(N) bend, CH_2(N) bend
653	37	654	Ring op asym bend
		600	Ring ip sym bend

With [EMIM][DEP], the diethylphosphate anion also has several vibrational modes that were detected by infrared spectroscopy. The stretching vibration of the P=O group is reported to be strong and in the region of 1350-1150 cm^{-1} and therefore the strong vibration at 1243 cm^{-1} is assigned to this functional group.[1] The assignment is also in agreement with previous studies of the diethylphosphate anion.[2] The symmetric PO_2^- stretch appears at 1082 cm^{-1}. P-O-C vibrations give very strong bands between 1050-970 cm^{-1} with another additional strong band typically between 985 and 940 cm^{-1}.[1] The very strong bands at 1049 cm^{-1} and 933 cm^{-1} are thus assigned to the P-O-C asymmetric stretching vibration. The symmetric P-O-C vibrations also typically exhibit strong bands between 830-740 cm^{-1},[1] so the band at 776 cm^{-1} is assigned to this mode.

Table S2. IR and Raman bands of [EMIM][MeSO$_3$] and their vibrational assignments. Asym = antisymmetric, sym = symmetric, str = stretch, ip = in-plane, op = out-of-plane, sh = shoulder.

Table S2 (continued). IR and Raman bands of [EMIM][MeSO$_3$] and their vibrational assignments. Asym = antisymmetric, sym = symmetric, str = stretch, ip = in-plane, op = out-of-plane, sh = shoulder.

Infrared (cm^{-1})	Relative Intensity	Raman (cm^{-1})	Vibrational assignment
		3161	Ring HCCH asym str
3148	14		Ring HCCH sym str
3094	26	3100	CH_3(N) HCH asym str
3038	17sh		SCH_3 asym astr
3008	15		SCH_3 sym str
2986	14	2965	CH_2HCH asym str
2938	10	2935	Terminal CH_3 HCH asym str
2881	6	2890	Terminal CH_3 HCH sym str
2832	3	2834	?
		2760	?
1635	8		?
1571	33	1569	C=N str
1467	17	1477	Ring ip asym str, CH_3(C) str
1456	17	1455	CCH HCH asym bend, CH_3(N) HCH sym bend
1426	14	1425	SO_2 asym str or CH_3 asym deform
1389	11	1389	Ring ip asym str, CH_2(N) bend
1359	10		Ring ip sym str, CH_2(N) and CH_3(N) str
1329	19	1337	Ring ip sym str, CH_2(N) str
1310	12sh		CH_3 sym deform
		1256	SO_2^- asym str
1198	98	1204	SO_2^- sym str
1176	100	1170	Ring ip asym str, CC str, (N)CH_2 and (N)CH_3CN str
1123	33sh		SOH bend
		1092	SO_2^- sym str
1038	89sh	1041	SCH_3 rocking
		1024	SO_3 sym str
963	12	960	CC str
873	23		SO str
847	25		SO str
806	23		CCH bend
765	77		CS str
702	18	702	Ring HCCH sym bend
649	36	651	Ring op asym bend
		599	Ring ip sym bend
		553	SO_3 sym bend
		527	SO_3 asym bend

Several of the vibrational characteristics of the [EMIM]$^+$ cation in [EMIM][MeSO$_3$] resembled that of [EMIM][DEP] with some exceptions. The CH_3(N) HCH asymmetric stretch for [EMIM][MeSO$_3$] appeared at 3094 cm^{-1} relative to 3046 cm^{-1} for [EMIM][DEP] because of reduced influence from the less basic [MeSO$_3$]$^-$ anion relative to [DEP]$^-$. In previous studies of methanesulfonic vibrations, the SO_2 asymmetric and symmetric stretching modes appear in the regions 1357-1467 cm^{-1} and 1140-1200 cm^{-1}, respectively[3, 4], so the vibration observed at 1426 cm^{-1} is assigned to the SO_2 asymmetric stretch and 1198 cm^{-1} to the symmetric stretch in [MeSO$_3$]$^-$. The shoulder at 1310 cm^{-1} is assigned to the CH_3 symmetric deformation of MeSO$_3$.[3, 4] Increasing the temperature from 298 K to 353 K resulted in a shift of the SCH_3 rocking mode to 1030 cm^{-1} and the CS stretch to 750 cm^{-1}.

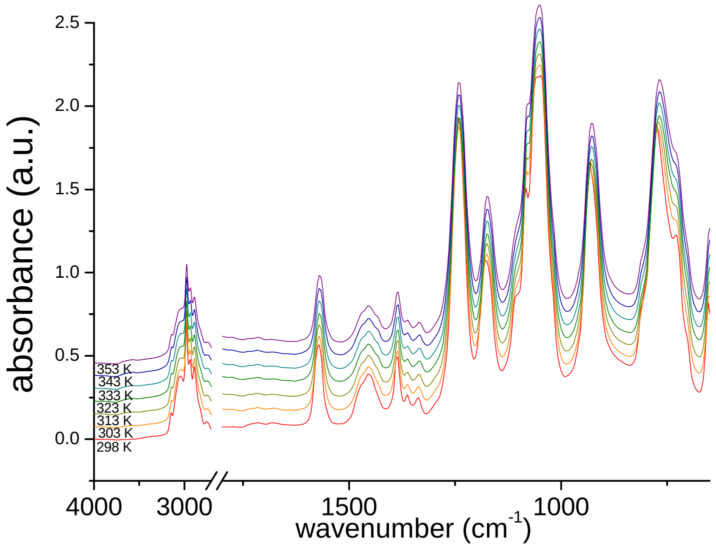

Figure S2: In-Situ ATR-IR spectra of [EMIM][DEP] measured at (—) 298 K, (—) 303 K, (—) 313 K, (—) 323 K, (—) 333 K, (—) 343 K, and (—) 353 K.

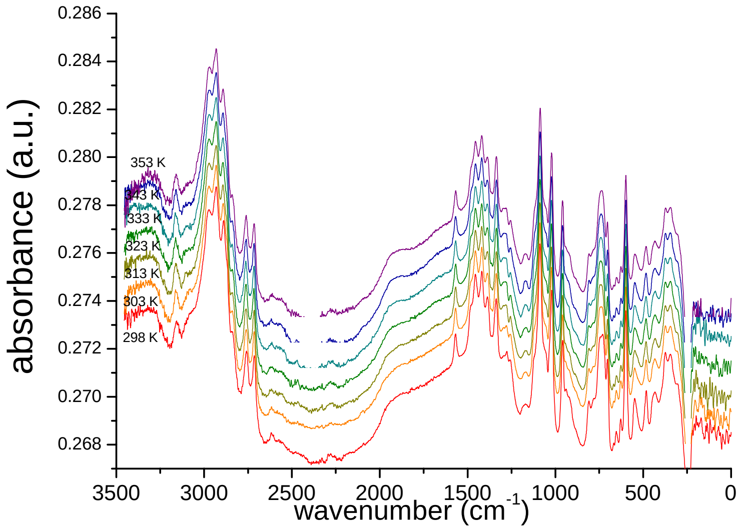

Figure S3: In-Situ Raman spectra of [EMIM][DEP] measured at (—) 298 K, (—) 303 K, (—) 313 K, (—) 323 K, (—) 333 K, (—) 343 K, and (—) 353 K.

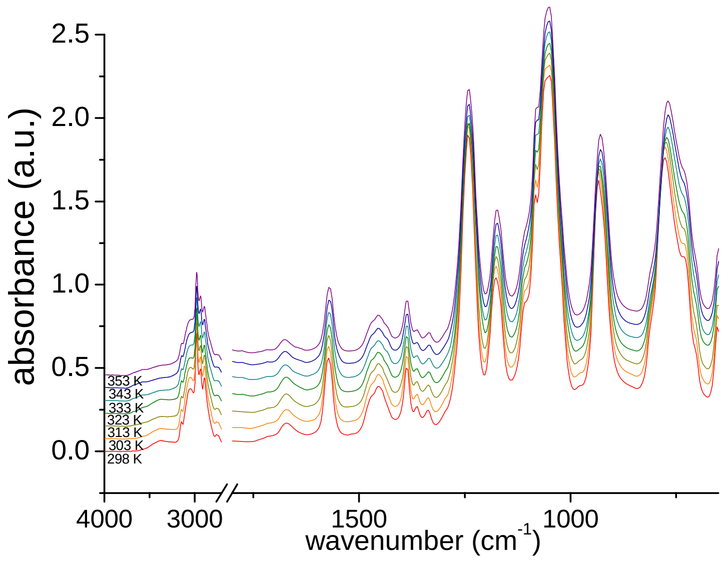

Figure S4: In-Situ ATR-IR spectra of [EMIM][DEP]/OH measured at (—) 298 K, (—) 303 K, (—) 313 K, (—) 323 K, (—) 333 K, (—) 343 K, and (—) 353 K.

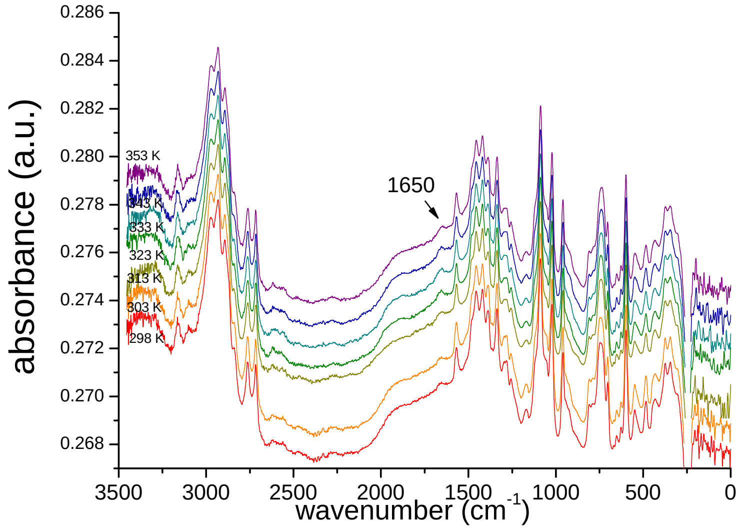

Figure S5: In-Situ Raman spectra of [EMIM][DEP]/OH measured at (—) 298 K, (—) 303 K, (—) 313 K, (—) 323 K, (—) 333 K, (—) 343 K, and (—) 353 K.

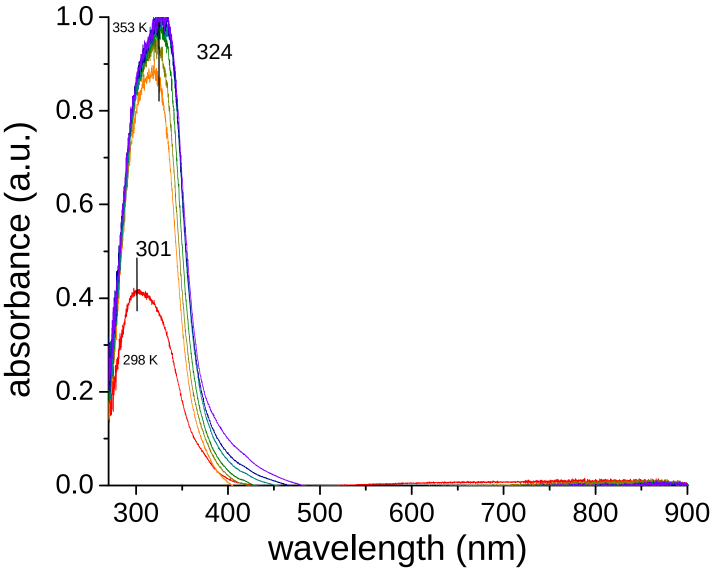

Figure S6: In-Situ UV-vis spectra of [EMIM][DEP]/OH measured at (—) 298 K, (—) 303 K, (—) 313 K, (—) 323 K, (—) 333 K, (—) 343 K, and (—) 353 K.

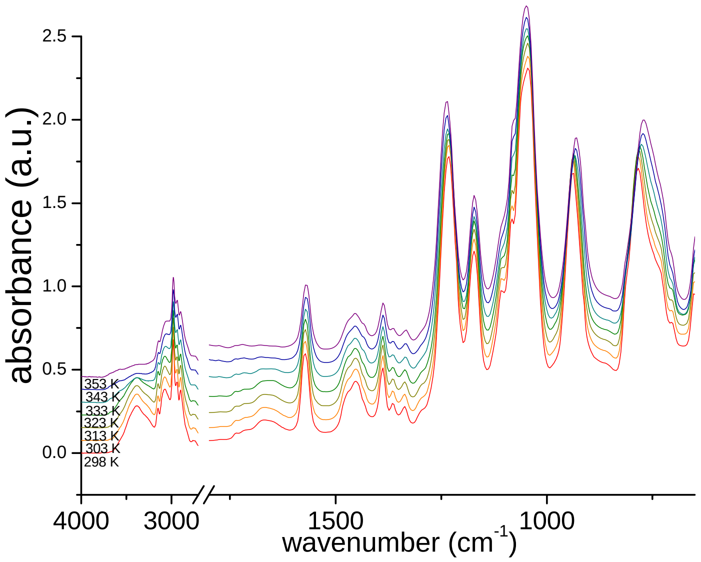

Figure S7: In-Situ ATR-IR spectra of Co/[EMIM][DEP] measured at (—) 298 K, (—) 303 K, (—) 313 K, (—) 323 K, (—) 333 K, (—) 343 K, and (—) 353 K.

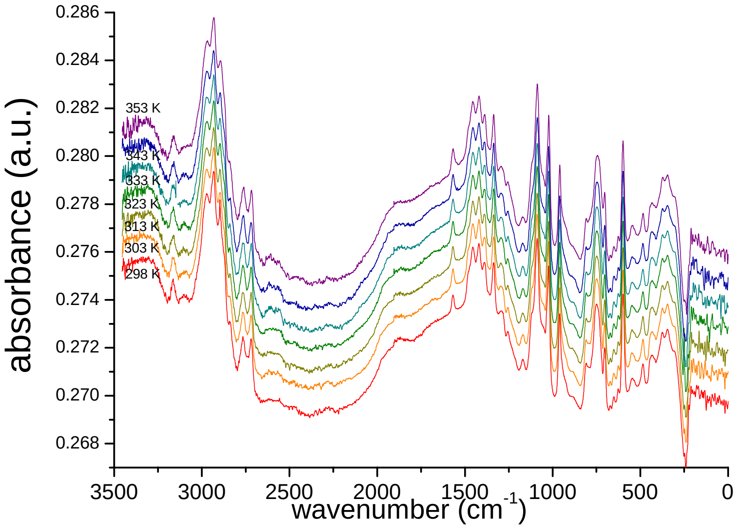

Figure S8: In-Situ Raman spectra of Co/[EMIM][DEP] measured at (—) 298 K, (—) 303 K, (—) 313 K, (—) 323 K, (—) 333 K, (—) 343 K, and (—) 353 K.

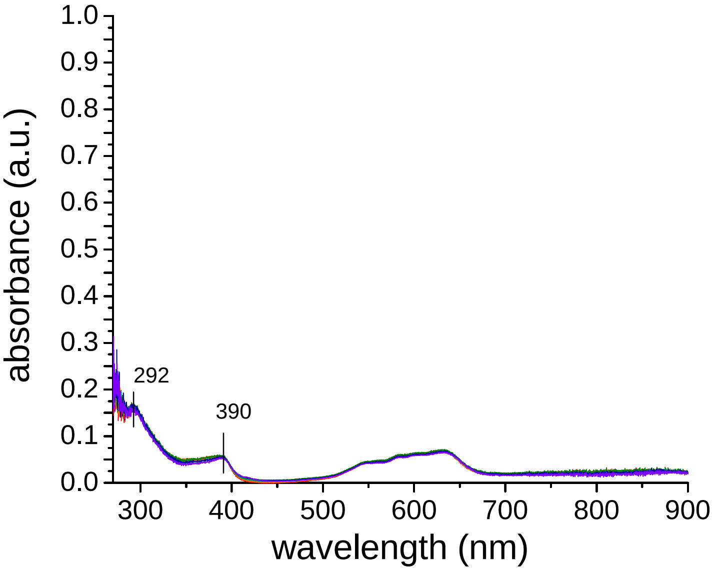

Figure S9: In-Situ UV-Vis spectra of Co/[EMIM][DEP] measured at (—) 298 K, (—) 303 K, (—) 313 K, (—) 323 K, (—) 333 K, (—) 343 K, and (—) 353 K.

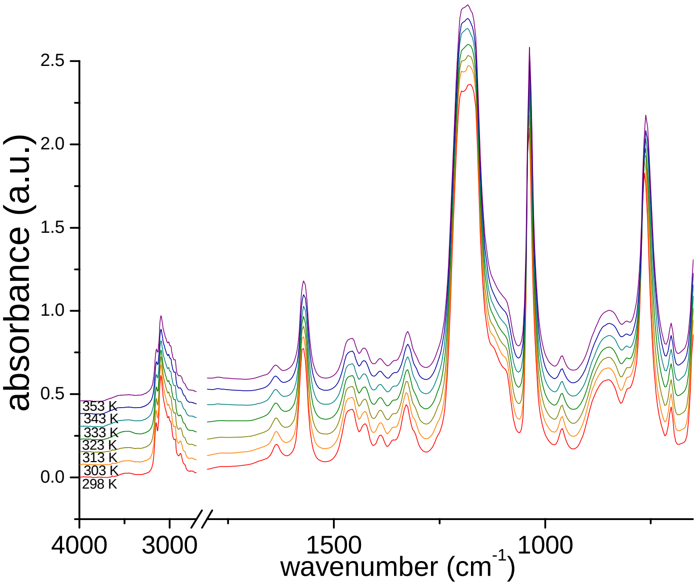

Figure S10: In-Situ ATR-IR spectra of [EMIM][$MeSO_3$] measured at (—) 298 K, (—) 303 K, (—) 313 K, (—) 323 K, (—) 333 K, (—) 343 K, and (—) 353 K.

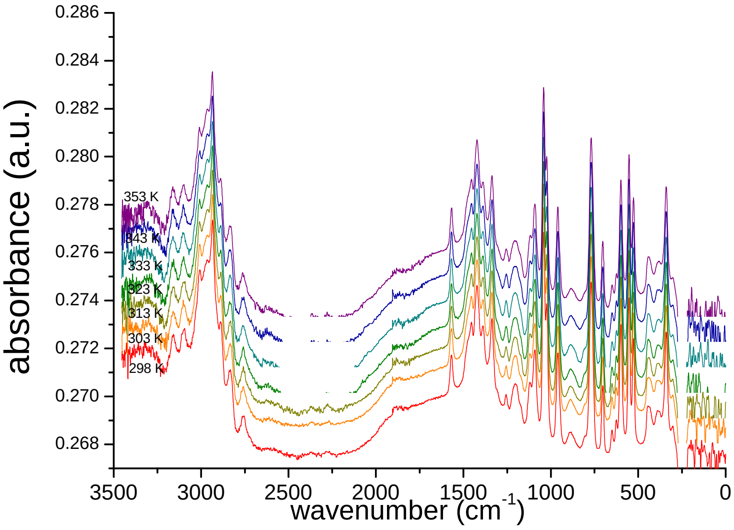

Figure S11: In-Situ Raman spectra of [EMIM][$MeSO_3$] measured at (—) 298 K, (—) 303 K, (—) 313 K, (—) 323 K, (—) 333 K, (—) 343 K, and (—) 353 K.

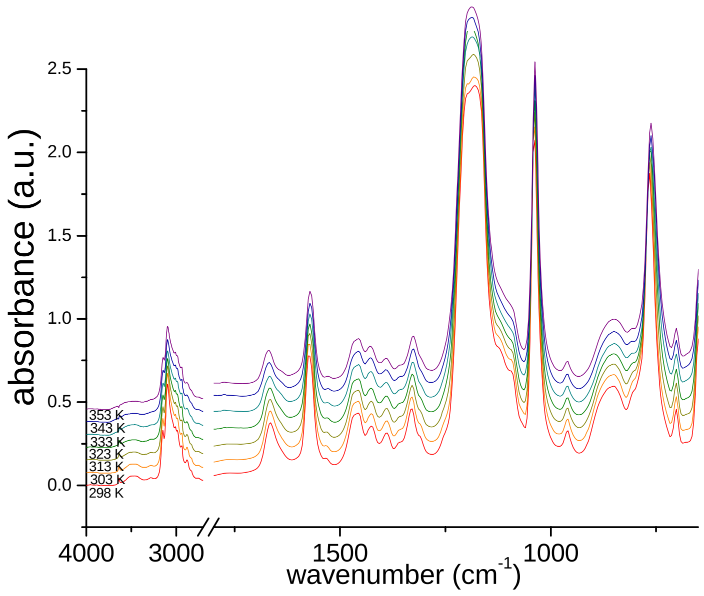

Figure S12: In-Situ ATR-IR spectra of [EMIM][MeSO$_3$]/OH measured at (—) 298 K, (—) 303 K, (—) 313 K, (—) 323 K, (—) 333 K, (—) 343 K, and (—) 353 K.

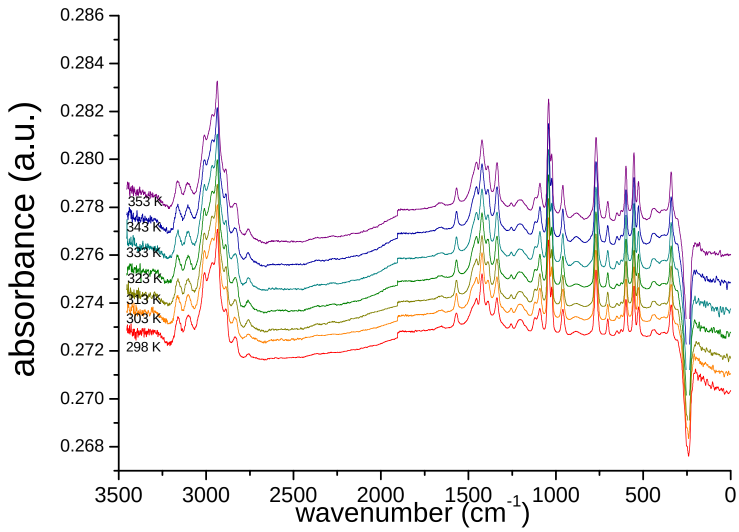

Figure S13: In-Situ Raman spectra of [EMIM][MeSO$_3$]/OH measured at (—) 298 K, (—) 303 K, (—) 313 K, (—) 323 K, (—) 333 K, (—) 343 K, and (—) 353 K.

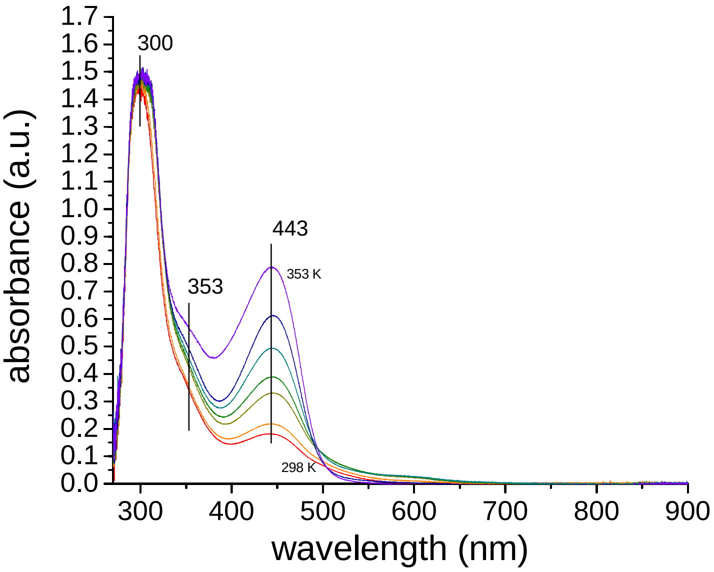

Figure S14: In-Situ UV-vis spectra of [EMIM][MeSO$_3$]/OH measured at (—) 298 K, (—) 303 K, (—) 313 K, (—) 323 K, (—) 333 K, (—) 343 K, and (—) 353 K.

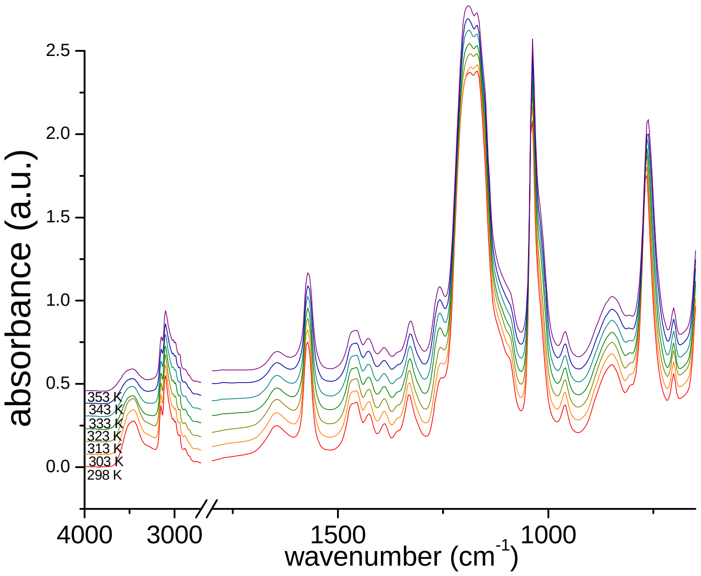

Figure S15: In-Situ ATR-IR spectra of Co/[EMIM][MeSO$_3$] measured at (—) 298 K, (—) 303 K, (—) 313 K, (—) 323 K, (—) 333 K, (—) 343 K, and (—) 353 K.

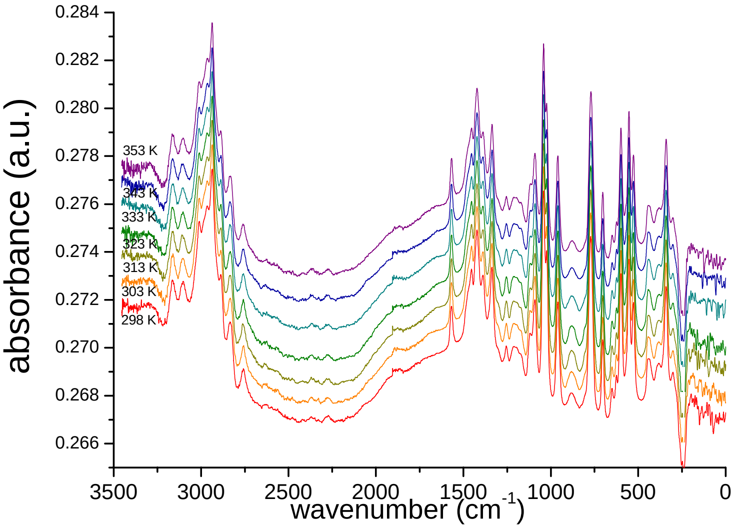

Figure S10: In-Situ Raman spectra of Co/[EMIM][MeSO$_3$] measured at (—) 298 K, (—) 303 K, (—) 313 K, (—) 323 K, (—) 333 K, (—) 343 K, and (—) 353 K.

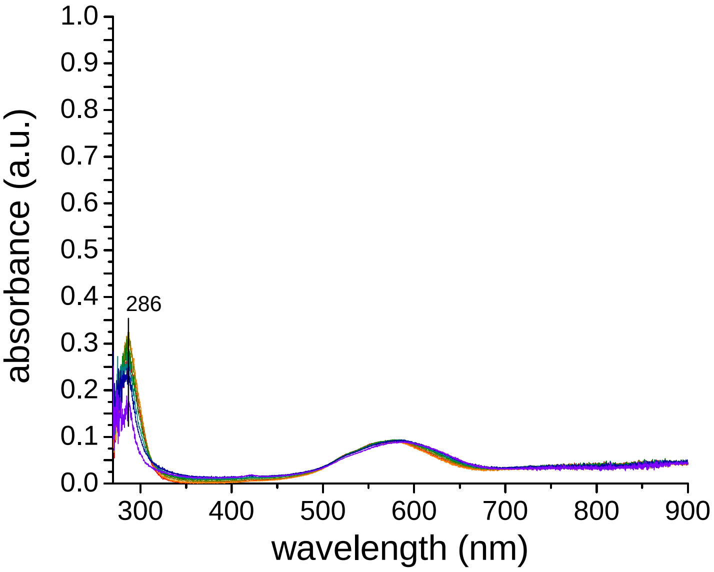

Figure S17: In-Situ UV-Vis spectra of Co/[EMIM][MeSO$_3$] measured at (—) 298 K, (—) 303 K, (—) 313 K, (—) 323 K, (—) 333 K, (—) 343 K, and (—) 353 K.

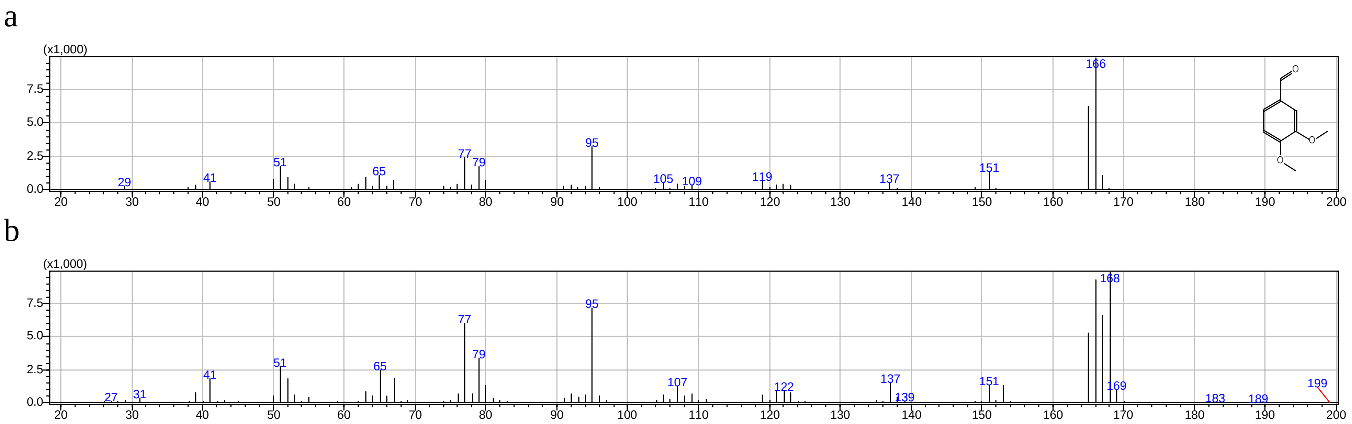

Figure S18: Mass spectra of a) veratraldehyde and b) veratraldehyde produced via Co/[EMIM][DEP]/OH catalyzed veratryl alcohol oxidation using $^{18}O_2$.

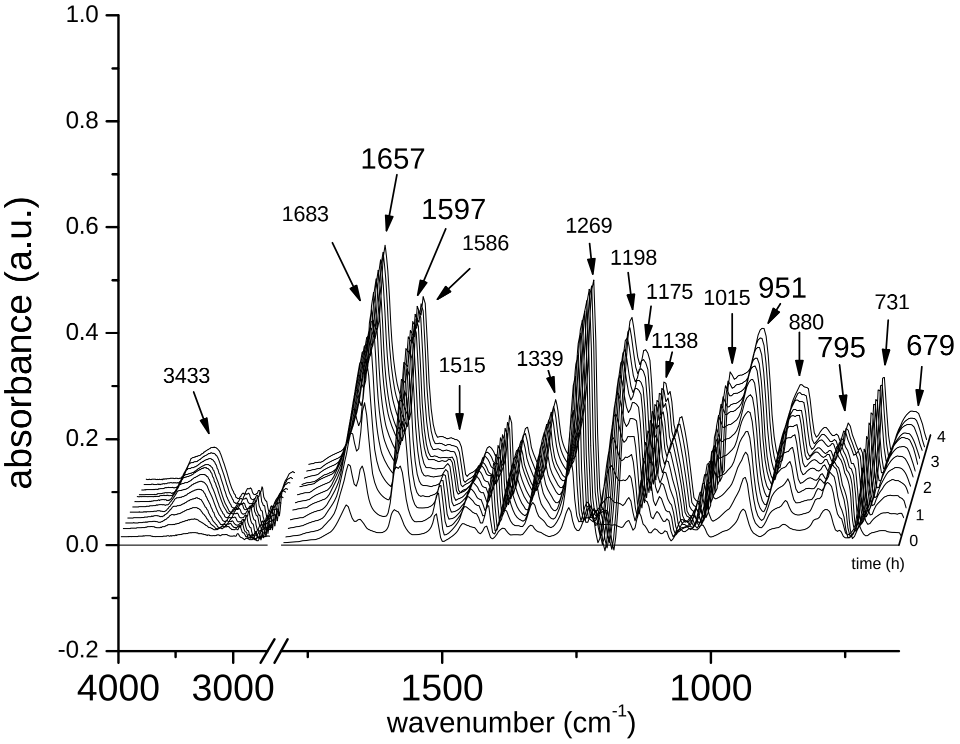

Figure S19: Reproduction of Figure 1 using $^{18}O_2$ as the oxidant.

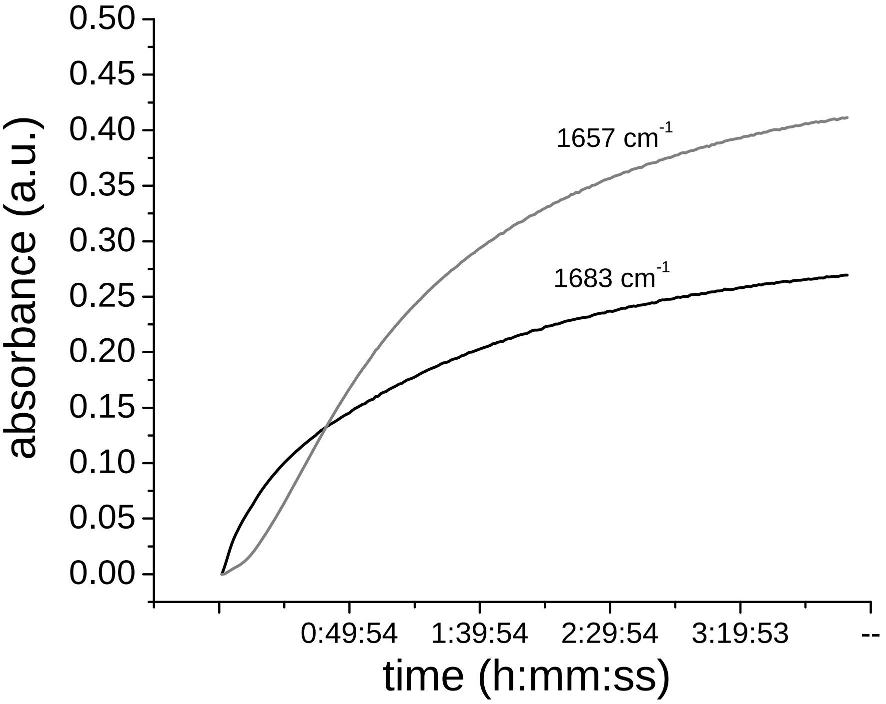

Figure S20. Vibrational intensities associated with ^{16}O (1683 cm^{-1}) and ^{18}O (1657 cm^{-1}) labelled veratraldehyde versus time using $^{18}O_2$ as the oxidant. Initially, only the ^{16}O veratraldehyde is observed. Each catalytic turnover (see Scheme S1) results in the formation of $H_2{}^{18}O_2$, which disproportionates to form $H_2{}^{18}O$. This $H_2{}^{18}O$ reacts with veratraldehyde to form a diol, and the reverse reaction results in either the formation of ^{16}O or ^{18}O labelled veratraldehyde. As the reaction proceeds, $H_2{}^{18}O$ concentrations increase, which results in increased incorporation of ^{18}O in the veratraldehyde as observed by the eventual increase in vibrational intensity at 1657 cm^{-1}.

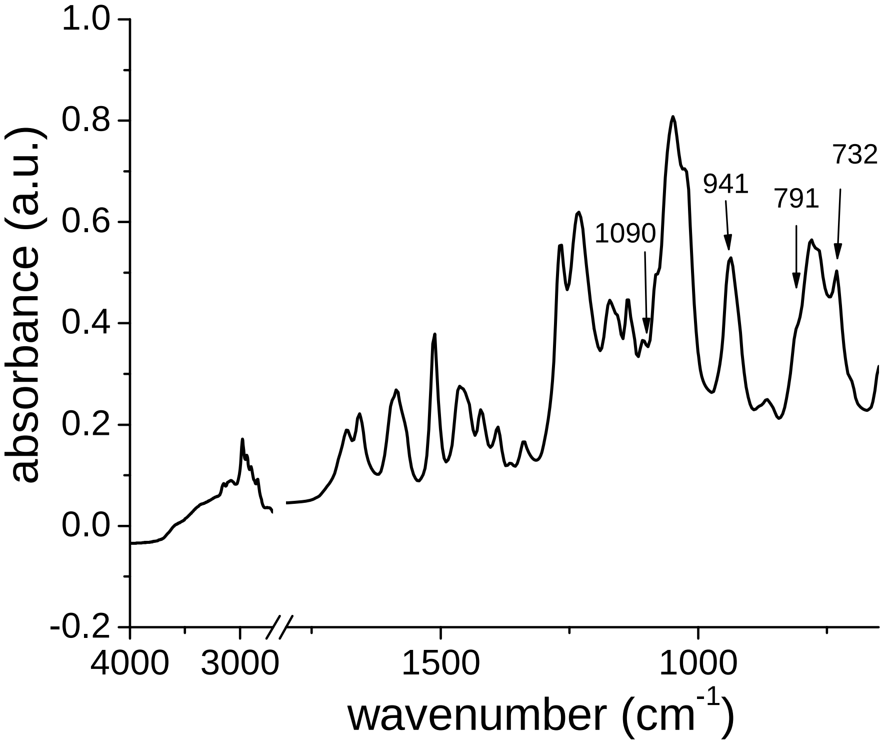

Figure S21: In-situ IR spectrum of Co/[EMIM][DEP]/OH catalyzed veratryl alcohol oxidation using $^{18}O_2$ for comparison with Figure 2. Vibrations associated with cobalt complexes are marked with arrows.

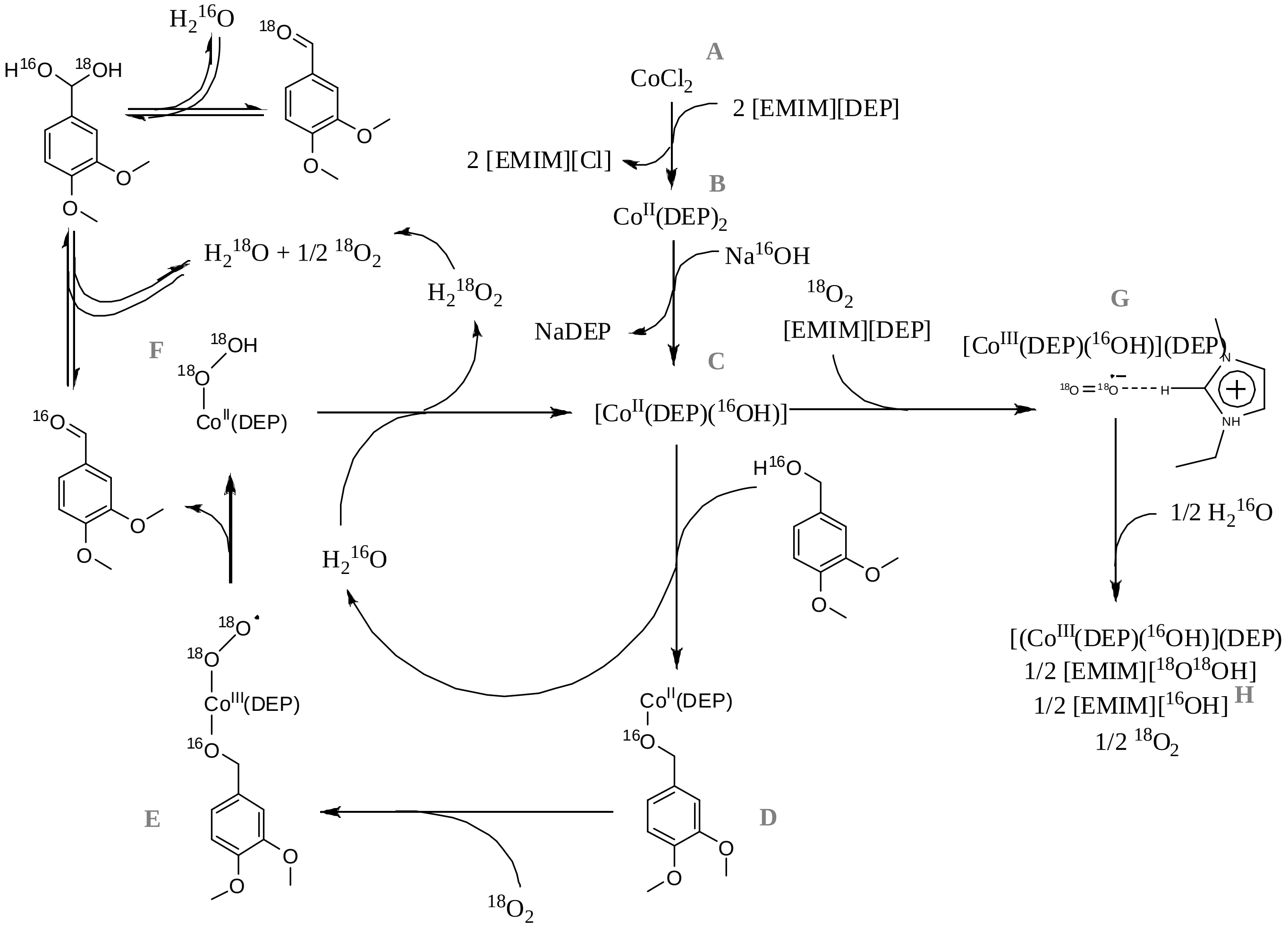

Scheme S1: Proposed catalytic mechanism depicting the exemplary oxidation of veratryl alchol to veratraldehyde in the ionic liquid [EMIM][DEP] using $^{18}O_2$ as the oxidant. The mechanism clearly indicates the mix of ^{16}O and ^{18}O-labelled veratraldehyde.

Supporting Information References

1 G. Socrates, *Infrared and Raman characteristic group frequencies: tables and charts*, Wiley, New York, 2001.

2 L. Azéma, S. Ladame, C. Lapeyre, A. Zwick and F. Lakhdar-Ghazal, *Spectrochim. Acta, Pt. A: Mol. Spectrosc.*, 2005, **62**, 287-292.

3 M. E. Tuttolomondo, A. Navarro, T. Pena, E. L. Varetti, S. F. Parker and A. B. Altabef, *J. Phys. Chem. A*, 2009, **113**, 8401-8408.

4 A. Givan, A. Loewenschuss and C. J. Nielsen, *J. Mol. Struct.*, 2005, **748**, 77-90.